IEEE Photonics Journal
An IEEE Photonics Society Publication

Open Access

High-Power High-Repetition-Rate Tunable Yellow Light Generation by an Intracavity-Frequency-Doubled Singly Resonant Optical Parametric Oscillator

Volume 12, Number 3, June 2020

Bing Sun
Xin Ding
Yuntao Bai
Xuanyi Yu
Yang Liu
Jingbo Wang
Lei Zhao
Tengteng Li
Guoxin Jiang
Peng Lei
Liang Wu
Guizhong Zhang
Jianquan Yao

DOI: 10.1109/JPHOT.2020.2994229

IEEE photonics SOCIETY

IEEE

High-Power High-Repetition-Rate Tunable Yellow Light Generation by an Intracavity-Frequency-Doubled Singly Resonant Optical Parametric Oscillator

Bing Sun,[1,2] Xin Ding ,[1,2] Yuntao Bai,[1,2] Xuanyi Yu,[3] Yang Liu,[1,2] Jingbo Wang,[1,2] Lei Zhao,[1,2] Tengteng Li,[1,2] Guoxin Jiang,[1,2] Peng Lei,[1,2] Liang Wu,[1,2] Guizhong Zhang,[1,2] and Jianquan Yao[1,2]

[1]School of Precision Instrument and Opto-Electronics Engineering, Institute of Laser and Opto-Electronics,Tianjin University, Tianjin 300072, China
[2]Key Laboratory of Opto-electronics Information Technology, Ministry of Education, Tianjin University, Tianjin 300072, China
[3]College of Physics Science, Nankai University, Tianjin 300071, China

DOI:10.1109/JPHOT.2020.2994229

Manuscript received March 11, 2020; revised May 5, 2020; accepted May 8, 2020. Date of publication May 12, 2020; date of current version May 20, 2020. This work was supported in part by the National Natural Science Foundation of China under Grants 11674242 and 11674243 and in part by Marine S&T Fund of Shandong Province for Pilot National Laboratory for Marine Science and Technology (Qingdao) under Grant 2018SDKJ0102-6. Corresponding author: Xin Ding (e-mail: dingxin@tju.edu.cn).

Abstract: An efficient intracavity-frequency-doubled singly resonant optical parametric oscillator (SR-OPO), pumped by a high-maturity 532 nm laser, tunable in the yellow wavelength region is demonstrated. An elaborate V-shaped idler cavity design is employed for a potassium titanyl phosphate (KTP) OPO nonlinear crystal to achieve a 5.06 W idler output at 1151.2 nm at a 10 kHz pulse repetition frequency. Using a second KTP crystal to intracavity frequency double the circulating idler wave, a 2.37 W yellow output at 575.6 nm is generated. High optical conversion efficiency (25.4% and 11.2%), 0.5 nm spectral linewidth, and 32 ns pulse duration of the 575.6 nm yellow output are achieved.

Index Terms: Singly resonant optical parametric oscillator, KTP crystal, High repetition rate, Intracavity frequency doubling, Yellow light.

1. Introduction

Coherent radiations in the yellow-orange wavelength range of 560–600 nm and blue-green wavelength range of 450–500 nm are of great importance in applications such as adaptive optics, spectroscopy, nuclear physics, underwater communication and bioluminescence detections [1]–[6]. Most laser frequencies in this region can be obtained by means of laser diode (LD)-pumped rare-earth-ion-doped lasers (Pr^{3+}, Tb^{3+}) [7], all-solid-state frequency-doubling and sum-frequency-mixing Nd^{3+}-doped lasers [8]–[10], all-solid-state or fiber Raman lasers [11]–[14], dye lasers [15], and optical parametric oscillators (OPOs) [16]–[24]. Output power of only several watts has been reported for Pr^{3+}-doped lasers, significantly below that of typical Nd^{3+}-doped lasers. Combined with second-harmonic generation (SHG), sum-frequency generation (SFG), or stimulated Raman scattering (SRS), Nd^{3+}-doped lasers can achieve an output power of tens or even hundreds of watts at several specific wavelengths. Even in terms of the narrow linewidth, a commercial 20-W sodium

guide star laser at 589 nm based on resonant frequency doubling of an infrared DFB diode laser with subsequent Raman fiber amplifier has been designed for astronomical adaptive optics control in ground-based telescopes at European Southern Observatory (ESO) in Chile, with a spectral width of 5 MHz [25]. However, there are still various requirements for wavelengths in different applications. For example, the use of sunlight's Fraunhofer lines in the blue-green and yellow-orange regions (H-β line at 486.13 nm, Na line at 589.59 nm) helps improve the signal-to-noise ratio of lidar during daytime detection [3]. Underwater communication and detection require an optimal wavelength with the lowest transmission loss, which depends on the characteristics of different water bodies [4]. Atomic vapor laser isotope separation (AVLIS) technology requires several wavelengths of narrow-linewidth yellow-orange lasers to achieve isotope separation [5]. In biofluorescence detection, the sensitivity of fluorochromes can be several-fold improved by the appropriate laser wavelength [6]. These required wavelengths cannot be achieved directly by the lasers described above, but only by tunable lasers such as dye lasers and OPOs. Owing to their high gain and large gain bandwidth, dye lasers are currently the main method of generating high-power and tunable visible light. However, the structures of dye lasers are complex and the maintenance is somewhat inconvenient. Compared with dye lasers, singly resonant OPOs (SR-OPOs) have some advantages in terms of structure and stability. The development of high-performance nonlinear crystals and solid-state pump sources has greatly improved the conversion efficiency of SR-OPOs [16]. Hence, SR-OPOs are currently the optimal choice for generating high-power tunable yellow-orange and blue-green light [17].

The power and efficiency of SR-OPOs depend on the pump intensity and the effective nonlinear coefficient (deff) of the crystals. However, the pump intensity is always limited by the damage threshold of the crystal, and it is hard to obtain a high damage threshold together with a large effective nonlinear coefficient. For continuous-wave (CW) OPOs in the yellow-orange and blue-green region, periodically-poled near stoichiometric $LiNbO_3$ (PPLN) or $LiTaO_3$ (PPLT) with a lower damage threshold and larger deff are used, with a low-to-moderate pump power. Together with the tight focusing of a single-frequency pump, a lower pump threshold and higher conversion efficiency can be achieved [16], [18]. In contrast, pulsed OPOs in this region can achieve much more nonlinear gain owing to the high peak intensity of pump light at a pulse repetition frequency (PRF) of 1–100 Hz. Therefore, nonlinear crystals with high damage threshold are preferred, although their deff are always lower, leading to a higher pump threshold of OPOs [19], [20]. However, for the high-repetition-rate operation of SR-OPOs, it is difficult to reach such a high pump threshold due to the limited pump intensity. Hence, the balance between pump intensity and deff of the crystals is an important problem that needs to be solved in order to achieve a high-power and high-repetition-rate SR-OPO in the yellow-orange and blue-green regions.

High-repetition-rate SR-OPOs in the yellow-orange and blue-green regions pumped by 532 nm or 355 nm lasers have been demonstrated. In 2018, Rao et al. demonstrated a type-I phase-matched β-BaB_2O_4 (BBO) crystal-based OPO at a PRF of 5 kHz, which is the highest PRF reported for visible OPOs pumped by a 355 nm laser [21]. By using cylindrical focusing of the pump beam, the threshold pump pulse energy is reduced to 1 mJ. The SR-OPO could be tuned within 490–630 nm and delivered 2.6 W output at 492 nm, with a UV to visible efficiency of 26%. In 2004, a green pumped lithium triborate (LBO)-OPO tunable in 924–970 nm was demonstrated by Li et al. [22]. Noncritical phase matching was adopted to avoid the walk-off in the 50-mm-long nonlinear crystal, and a double-pass pump scheme with a beam quality of 3 was used to lower the threshold of the OPO (29 MW/cm^2). A maximum average output power of 9.3 W was obtained at a PRF of 10 kHz and a pump power of 18 W, with a conversion efficiency of 54%. Using three bismuth borate (BIBO) crystals to extra-cavity frequency-double the signal output, 1.3 W of 470 nm output was obtained [23].

Compared with 355 nm pumped OPOs, the 532 nm green pumped OPOs usually involve another frequency-doubling process of the idler or signal wave to obtain the yellow-orange or blue-green output, which limits the optical efficiency to some extent. However, the third-harmonic generation process to generate 355 nm also limits overall efficiency, and the dielectric coatings on mirrors and crystals are usually less resistant to the 355 nm ultraviolet, which could result in worse stability

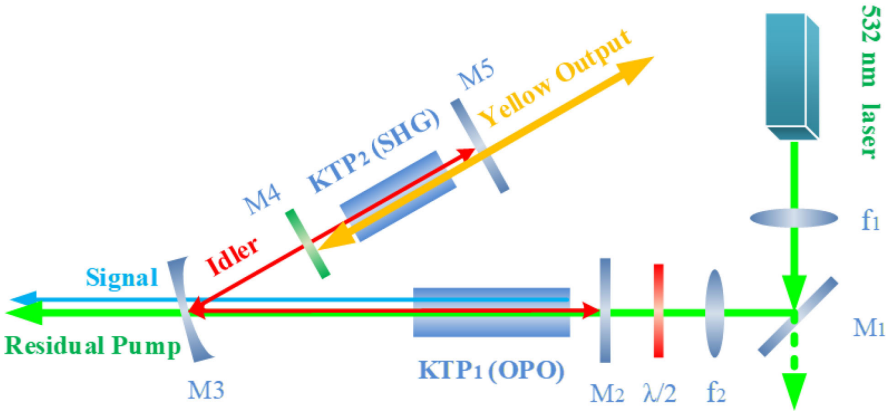

Fig. 1. Schematic of the green-pumped singly resonant optical parametric oscillator (SR-OPO). M: mirror; f: focusing lens; and KTP: potassium titanyl phosphate crystal.

than the green-pumped OPOs. High-repetition-frequency 532 nm green laser is more mature than 355 nm, and the corresponding OPO crystal options are more diverse, including potassium titanyl phosphate (KTP), PPLN, PPLT, LBO, etc. PPLN and PPLT crystals are not commonly used in high-power nanosecond-pulses OPO due to low damage threshold. Currently, most of the high-power high-repetition-frequency green-pumped OPOs have used LBO crystals with a high damage threshold and small walk-off as the nonlinear gain media, because the drawback of the relatively low deff can be compensated by higher pump intensity, better beam quality, and longer interaction length. In fact, a nonlinear crystal with larger deff (such as KTP) relaxes the requirements for the pump source appropriately, and allows the OPO to operate efficiently with a lower pump intensity just below the damage threshold. In our experiment, a gray-trace resistance KTP crystal was selected as OPO crystal, due to the large deff and dimension, high damage threshold, and the weak walk-off effect which can be effectively controlled by adjusting the size of the beam. Moreover, compared to the extracavity frequency doubling, a high-efficiency intracavity-frequency-doubling process seems to be a better option to improve the overall efficiency for high-power and high-repetition-rate SR-OPOs in the yellow-orange or blue-green regions by elaborate cavity design. The KTP crystal was also selected as SHG crystal in our experiment, due to a larger acceptance angle.

In this paper, an efficient intracavity-frequency-doubled SR-OPO tunable in the yellow wavelength region is demonstrated. A KTP crystal is used as the nonlinear crystal considering the pump intensity and the deff of the crystal. An elaborate V-shaped cavity is adopted for the purpose of mode-matching and controlling the walk-off in the crystal, thus ensuring the conversion efficiency of the OPO. 5.06 W idler output at 1151.2 nm is obtained with a 532 nm pump power of 19.9 W at a PRF of 10 kHz, with a corresponding conversion efficiency of 25.4%. Using a second KTP crystal to intracavity frequency double the circulating idler wave, 2.37 W yellow output at 575.6 nm is generated. The green to yellow efficiency is 11.2%. The wavelength tuning range realized by rotating the two crystals is 573–578 nm. The wavelength coverage can be further extended to the whole orange-yellow region by cutting the KTP crystals at different angles. The device is also capable of achieving high-repetition-rate and high-power tunable blue-green light by changing the coating of the cavity mirror and the SHG crystal to intracavity frequency double the circulating signal wave.

2. Experimental Setup

The experiment setup is depicted in Fig. 1. The pump source of the OPO is a multi-mode frequency-doubled Nd:YAG laser at 532 nm, with a PRF of 10 kHz and a spectral linewidth of 0.1 nm ($M^2 =$

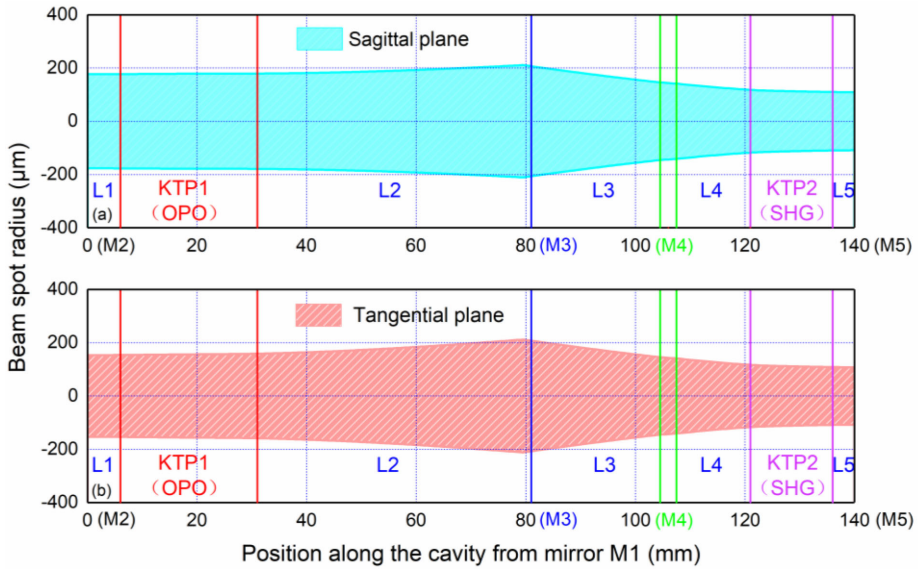

Fig. 2. Fundamental-mode beam size in (a) sagittal plane and (b) tangential plane.

$\sim$10). The pump light was focused onto a nonlinear crystal KTP1 by two focusing lens f1 and f2. A half-wave plate was used to rotate the polarization direction of the pump. A 7$\times$7$\times$25-mm^3 KTP crystal (KTP1) with an OPO acceptance bandwidth of $\sim$ 0.12 nm at 532 nm was cut at $\theta = 77°$, $\varphi = 0°$ for the type-II phase matching. Two facets of the crystal were coated to be anti-reflective (AR) at the 532 nm pump, 1120–1200 nm idler, and 950–1020 nm signal wavelengths. Considering the damage threshold of the crystal and the walk-off in it, the pump beam radius in the crystal was $\sim$300 μm. The V-shaped idler cavity of the SR-OPO consisted of a flat mirror M2, a concave folding mirror M3 with a radius of curvature of 100 mm, and a flat output coupler M5. Compared to four-mirror ring-cavity, the V-shape cavity has shorter cavity length and lower loss, and only one folding mirror is needed to focus the oscillating beams on the OPO crystal and SHG crystal, which is conducive to reducing astigmatism. More importantly, the double SHG process in the V-shape cavity actually shortens the length of SHG crystal, which is beneficial to suppress the beam walk-off effect. The half folding angle of M3 is $\sim$20°. M2 and M3 were coated to be AR at 532 nm (R$<$2%) and highly-reflective (HR) at the 1120–1200 nm idler frequency (R$>$98%). M5 served as the output coupler and was coated for HR at 1120–1200 nm (R$>$98%) and AR at 560–600 nm (R$<$2%). It should be noted that no mirrors are specifically coated for 950–1020 nm signal wave (T = 88-92%). Another KTP crystal, KTP2 (5$\times$5$\times$15 mm^3) cut at $\theta = 71.1°$, $\varphi = 0°$, was used to intracavity frequency double the circulating idler wave. The crystal was coated to be AR at 1120–1200 nm and 560–600 nm. Both KTP1 and KTP2 were wrapped in indium foil and placed in aluminum holders cooled at 18°C. A flat dichroic mirror M4 was placed between KTP2 and M3 to collect the backward-propagating yellow light.

Considering the crystal damage threshold, walk-off, and mode matching, the distance between each element were set as following: KTP1-M2 (L1): 6 mm; KTP1-M3 (L2): 50 mm; M3-M4 (L3): 23.5 mm; KTP2-M4 (L4): 13.5 mm; and KTP2-M5 (L5): 4 mm. The thickness of M4 is 3 mm with a refractive index of 1.516. The total length of the V-shaped idler cavity was 140 mm. Fig. 2 shows the fundamental-mode beam size of the idler in the cavity, calculated using the ABCD matrix. The sagittal and tangential beam radii in KTP1 were $\sim$180 and $\sim$160 μm, respectively. Such cavity arrangement and beam size are chosen for mode matching between the pump and the oscillator beam, as well as to avoid crystal damage and to minimize the influence of astigmatism induced by M3. The walk-off-limited maximum allowed interaction length l_a can be determined using the

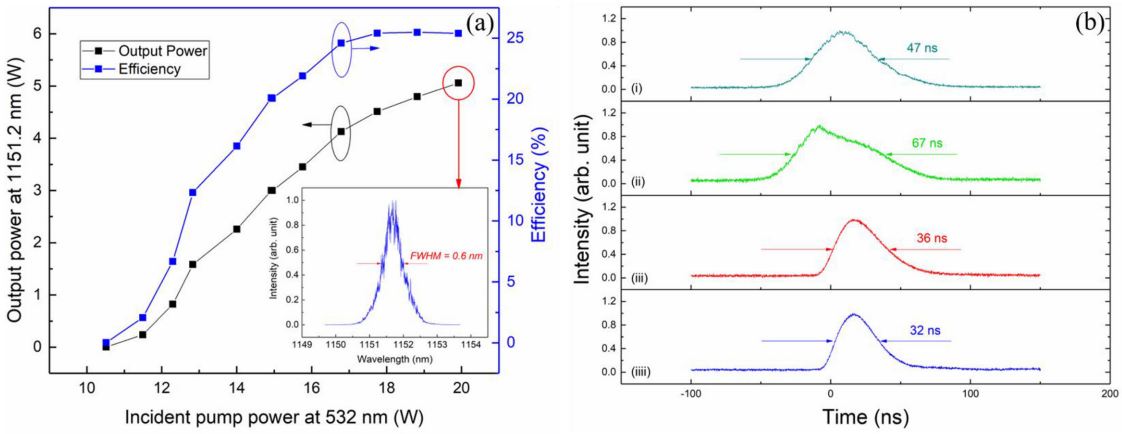

Fig. 3. (a) The power transfer of the idler output coupled optical parametric oscillator (OPO). Inset: Idler spectrum at the maximum power. (b) Oscilloscope traces of (i) incident pump, (ii) residual pump, (iii) 1151.2 nm idler wave, and (iiii) 989.6 nm signal wave.

following equation [19], [24]:

$$l_a = \frac{\sqrt{\pi}\omega_0}{\rho} \tag{1}$$

where ω_0 is the pump radius and ρ is the walk-off angle. For the type-II phase-matched KTP-OPO here, the walk-off angle ρ is calculated as ~23 mrad and the measured pump radius ω_0 is ~300 μm. Hence, the interaction length l_a is calculated to be ~23 mm, which is close to the actual crystal length of 25 mm. The beam radius of the fundamental-mode idler wave in KTP2 was ~110 μm, offering a high intensity of idler wave for efficient intracavity frequency doubling.

In the experiment, we also replaced the yellow output coupler M5 by an idler output coupler with different transmittance (T = 5%, 10%, 15%). Finally, the output coupler with T = 5% was determined as the optimal transmittance, due to the higher idler output power and conversion efficiency. The optical powers were measured by a laser power meter Ophir VEGA (sensor 12A). The full-width at half-maximum (FWHM) spectral linewidth of the near infrared idler output was measured using an optical spectrum analyzer (Yokogawa AQ6370D). Pulse shapes were recorded using an oscilloscope (Tektronix DSO9254A) and two fast photodiodes (Thorlabs DET08C and Thorlabs DET025A). Spectral linewidth of the yellow output was recorded using an optical spectrum analyzer (Ocean Optics HR4000) at the maximum power. The beam profile of the yellow output was recorded using a camera (Ophir Pyrocam III).

3. Results and Discussion

3.1. Near Infrared Idler Output at 1151.2 nm

We measured optical power with the yellow output coupler M5 replaced by an idler output coupler (T = 5%) to investigate the performance of the OPO, without KTP2 and M4. Fig. 3(a) plots the power transfer of the OPO with idler output. The OPO started oscillation at 10.5 W pump average power. After that, the conversion efficiency increased with the pump power until the pump power reached 17.7 W. The maximum idler average output power of 5.06 W was achieved at the pump power of 19.9 W, with corresponding conversion efficiency of 25.4%. The maximum signal power was also measured to be 3.95 W behind the folded mirror M3. The FWHM spectral linewidth of the idler wave was 0.6 nm at the maximum power, which was smaller than the acceptance bandwidth of KTP2 crystal (~ 0.85 nm) for frequency doubling of the 1151.2 nm.

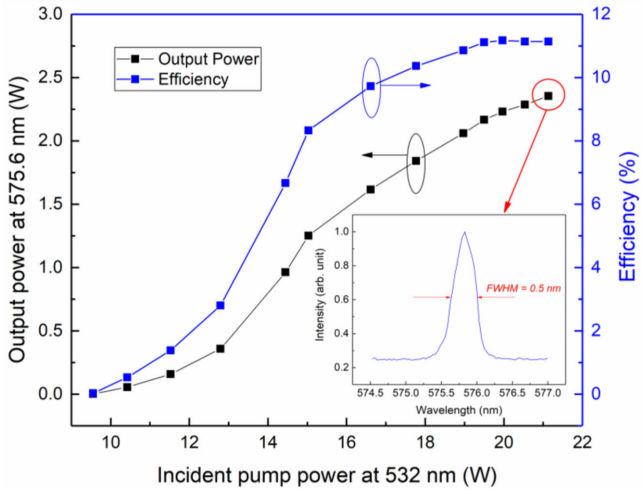

Fig. 4. The power transfer of the intracavity frequency-double optical parametric oscillator (OPO). Inset: Yellow output spectrum at the maximum power of 2.37 W.

The pulse shapes of the incident pump, residual pump, 1151.2 nm idler wave, and 989.6 nm signal wave are shown in Fig. 3(b). The pulse duration of the incident pump was 47 ns. Given the 160 mm optical length of the OPO cavity, the round-trip time of the idler wave in the cavity was 1.06 ns and one pump pulse duration allowed 45 round trips. Because the idler pulses started oscillating only when the pump intensity was higher than the OPO threshold, the buildup of idler pulse exhibited some delay compared with the pump pulse, resulting in an idler pulse duration of 36 ns, which is shorter than the recorded duration of the pump pulse. The pulse durations of the signal wave and the residual pump measured behind mirror M3 were 32 ns and 67 ns, respectively. It should be mentioned that at the moment when the signal and idler wave pulses were generated, the incident pump pulse started to be consumed continuously, corresponding to the maximum intensity of the residual pump. In addition, the pulse width of the residual pump was slightly broadened compared to the incident pump, due to a lower peak power.

3.2. Intracavity Frequency-Doubled Yellow Output

The yellow output coupler HR at idler wavelength and AR at yellow was used as M5, and the SHG crystal KTP2 and the dichroic mirror M4 were inserted into the cavity. With this arrangement, the yellow output (OPO) threshold was 9.5 W pump power, which was a bit lower than that with the T = 5% idler output coupled. The maximum yellow average output power was 2.37 W at 575.6 nm at the incident pump power of 21.1 W, with corresponding conversion efficiency of 11.2%. The equipment-resolution-limited spectral linewidth was 0.5 nm at the maximum power, as shown in Fig. 4.

It should be mentioned that the saturation of conversion efficiency occurred at a higher pump power of 19.5 W than that with the 5% idler output coupler. This is because the SHG process acts as an alterable nonlinear loss of the idler field in the intracavity frequency-doubled OPO, which is higher than that of the 5% idler output coupled. In order to explain the dynamics of intracavity frequency-doubled SROPO, simple models of OPO and SHG processes are employed under the plane-wave approximation. The OPO and SHG interactions are described by the equations [26]:

$$\frac{dE_s(z)}{dz} = i\frac{\omega_s}{n_s c} d_1 E_p(z) E_i^*(z) e^{i\Delta k_1 z} \tag{2}$$

$$\frac{dE_i(z)}{dz} = i\frac{\omega_i}{n_i c} d_1 E_p(z) E_s^*(z) e^{i\Delta k_1 z} \tag{3}$$

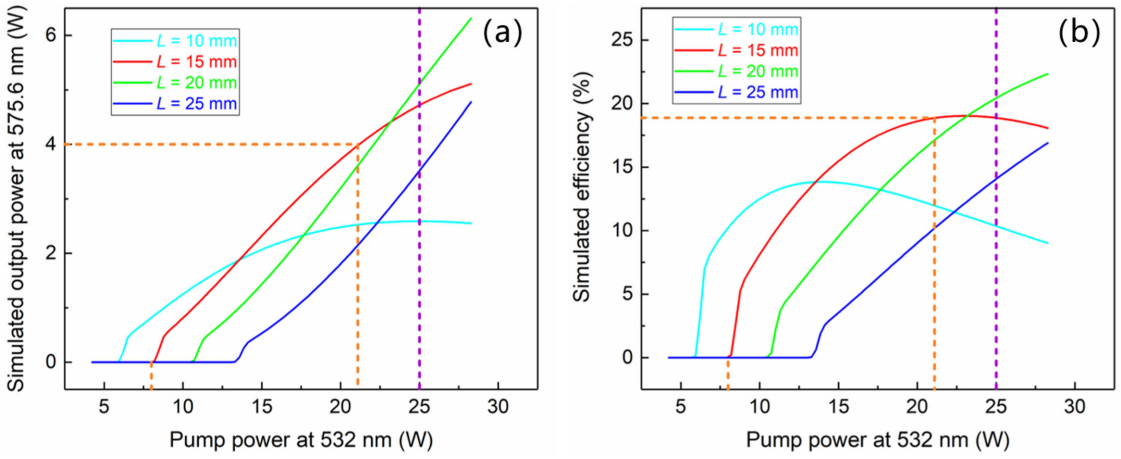

Fig. 5. (a) The simulated power transfer and (b) efficiency of the intracavity frequency-double OPO with different length of the SHG crystal (KTP2).

$$\frac{dE_p(z)}{dz} = i\frac{\omega_p}{n_p c} d_1 E_s(z) E_i(z) e^{i\Delta k_1 z} \tag{4}$$

$$\frac{dE_i(z)}{dz} = i\frac{\omega_i}{n_i c} d_2 E_d(z) E_i^*(z) e^{i\Delta k_2 z} \tag{5}$$

$$\frac{dE_d(z)}{dz} = i\frac{\omega_d}{n_d c} d_2 E_i^2(z) e^{i\Delta k_2 z} \tag{6}$$

The yellow output power can be calculated by the Runge-Kutta algorithm with the above equations, where *d1* and *d2* are the effective nonlinear coefficients of KTP1 and KTP2 crystals, respectively; $\Delta k1$ and $\Delta k2$ are the wave-vector mismatch of the OPO and SHG process, respectively; nj, $j = s, i, p, d$, are the refractive indices; Ej and ωj are the complex amplitudes and frequency of the electric-field, respectively. Fig. 5 shows the simulated power transfer and efficiency of the intracavity frequency-double OPO with different length of KTP2, respectively. As the length of KTP2 increases, the saturation of conversion efficiency occurs at a higher pump power, together with a higher pump threshold, which is similar to a SROPO with different transmittance output coupler. However, different from the output coupler with a certain transmittance, the SHG process acts as an alterable nonlinear loss of the circulating idler wave (formula 7). In order to better understand the dynamic process of intracavity frequency-doubled SROPO, we consider the steady state output characteristics of SROPO and SHG processes. Without considering other losses, the idler wave generated from the SRO process should be equal to the idler wave consumed in the SHG process to keep the intensity of the idler wave I_i in the cavity constant [27], [28]:

$$I_{P0} sin^2\left(\sqrt{\beta_{OPO} I_i} L_1\right) \frac{\omega_i}{\omega_p} = I_i tanh^2\left(\sqrt{\beta_{SHG} I_i} L_2\right) = I_{Yellow} \tag{7}$$

$$\beta_{OPO} = \frac{\mu_0 \omega_s \omega_p {d_1}^2}{2 n_s n_i n_p c}, \beta_{SHG} = \frac{\mu_0 {\omega_i}^2 {d_2}^2}{2 {n_i}^2 n_{2i} c} \tag{8}$$

$$\eta_{Yellow} = sin^2\left(\sqrt{\beta_{OPO} I_i} L_1\right) \frac{\omega_i}{\omega_p} = I_i tanh^2\left(\sqrt{\beta_{SHG} I_i} L_2\right) / I_{P0} \tag{9}$$

According to formula (9), the steady-state intensity of intracavity idler wave I_i can be solved with different pump intensity I_{p0} above the threshold. Furthermore, the output power and conversion efficiency of yellow light can also be solved. It can be found that the output power and conversion

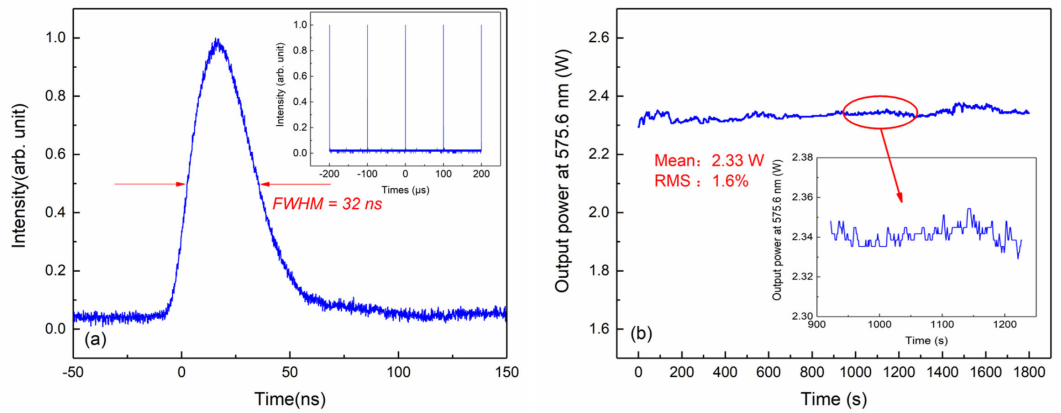

Fig. 6. (a) The oscilloscope trace of the 575.6 nm yellow output. Inset: The pulse train of the 575.6 nm yellow output. (b) The power stability of the 575.6 nm yellow output at the maximum power over 30 min. Inset: The power stability of the 575.6 nm yellow output at the maximum power over 5 min.

efficiency of yellow light mainly depend on the steady-state intensity of intracavity idler wave when other parameters are fixed, such as crystal length. However, according to formula (7), steady-state intensity of intracavity idler wave is related to the pump intensity and the parameters of OPO and SHG crystal. The phenomenon of efficiency saturation shows that steady-state intensity of intracavity idler wave cannot always increase with the increase of pump intensity. Moreover, for a certain pump power, there is an optimal length of KTP_2 (less than the interaction length l_a) to optimize yellow output power when the parameters of KTP_1 crystal are fixed. A 15 mm-long KTP crystal was preferred in the experiment, with the incident pump power lower than 25 W. It should be mentioned that the experimental yellow output power and efficiency are a little lower than that of simulation, together with a higher pump threshold, due to the neglect of the loss caused by mode mismatching and phase mismatching during the simulation.

The pulse duration of the yellow output was 32 ns, as shown in Fig. 6(a). The pulse train was also given in the inset of Fig. 6(a), demonstrating good pulse-to-pulse stability. Fig. 6(b) shows the power stability of the yellow output measured over 30 min, which exhibited a root-mean-square (RMS) fluctuation of 1.6%. Using a lens with a focal length of 100 mm to focus the yellow light at the maximum output power of 2.37 W, the beam quality M^2 factors of the 575.6 nm yellow output in the x and y directions was measured to be 3.0 and 3.1 by the knife-edge scanning. The beam profile is shown in the inset of Fig. 7(a). The beam radii of the idler and yellow light at KTP2 crystal were estimated to be $\sim$280 μm with the transmission formula of the gaussian beam, which indicated that the idler and yellow light were also multi-mode. In addition, it can be found that the beam quality of the yellow light is no worse than that of the multi-mode pump light ($M^2 = \sim 10$), which is different from that of the single-mode pump light [29]. This is probably because for multi-mode pump with relatively poor beam quality, the intensity from the center to the edge is more uniform. The back-conversion effect caused by the high center intensity is not obvious, which can lead to serious spatial distortion with single-mode pump light [30]. Meanwhile, the influence of multi-mode pump beam on the beam quality and output power of idler and yellow light can be further reduced by optimizing the mode matching between the idler and pump light with an elaborate V-shaped cavity design.

573–578 nm yellow output was realized by rotating the KTP1 crystal. During the process of wavelength tuning, the KTP2 crystal was simultaneously rotated for the highest SHG efficiency at different idler wavelengths. Further rotation of KTP1 would stop the OPO oscillating. Fig. 7(b) shows the tuning curve of the yellow output. The average power of the yellow output was higher than 1 W in the range of 574.1–577.1 nm. It should be mentioned that the above results were obtained without the re-optimization of the mirrors during the tuning process. This is because the

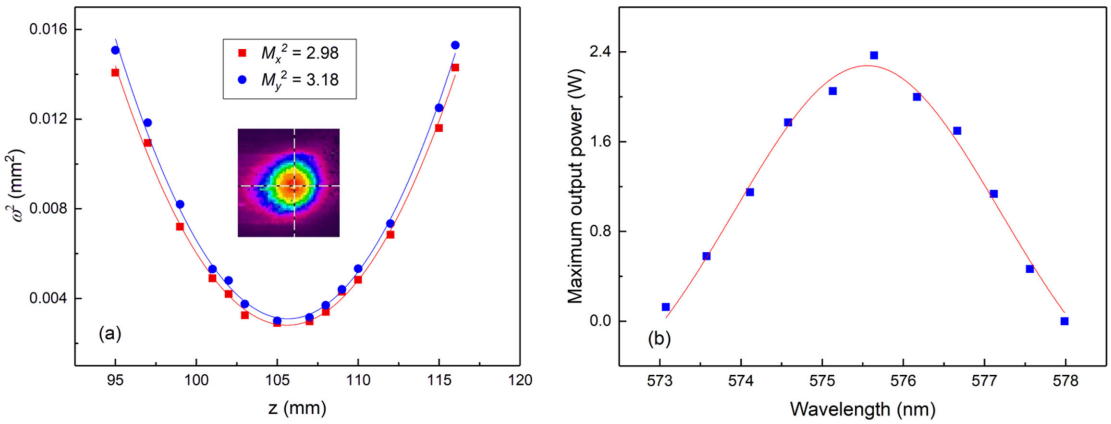

Fig. 7. (a) The beam quality measurement of the 575.6 nm yellow output at the maximum power of 2.37 W. Inset: The beam profile collected. (b) The tuning curve of the yellow output under the maximum pump power of 21.1 W.

excessive adjustment elements will increase the difficulty of cavity optimization. Therefore, the rotation of crystals may induce some cavity misalignment, as well as the phase mismatching, which decreases the conversion efficiency and output power at other wavelength. Actually, we have also tried to optimize the conversion efficiency by adjusting the mirrors while rotating the crystals for wavelength tuning. The maximum yellow output power we can get is slightly lower than that of 575.6 nm without any element rotation, due to the unavoidable loss of light deflection. This is in line with our expectation that adjusting the crystals and mirrors simultaneously is actually equivalent to replace the original KTP1 crystals with another cutting angle, neglecting the loss caused by light deflection. By using crystals with different cutting direction, the output wavelength of the OPO could cover the yellow-orange region. This KTP-OPO is also capable of delivering tunable blue-green output by using mirrors with corresponding coating and frequency-doubling the circulating signal wave.

4. Conclusion

In this work, an efficient intracavity frequency-doubled KTP-OPO with V-shaped idler cavity tunable in the yellow wavelength region is demonstrated. With an output coupling of 5%, 5.06 W idler output at 1151.2 nm was obtained at the pump power of 19.9 W with a PRF of 10 kHz. The corresponding optical conversion efficiency reaches 25.4%. By intracavity frequency-doubling the circulating idler field with another KTP crystal, yellow output tunable in 573–578 nm was realized. The maximum yellow average power was 2.37 W at 575.6 nm, at the maximum green pump power of 21.1 W, with a conversion efficiency of 11.2%. The yellow output exhibited a beam quality factor of $\sim$3 and an RMS fluctuation of 1.6% over 30 min. Moreover, the wavelength coverage can be further extended to the whole orange-yellow region by cutting the KTP crystals at different angles. The device is also capable of achieving high-repetition-rate and high-power tunable blue-green light by changing the coatings of the cavity mirrors and the SHG crystal to intracavity frequency double the circulating signal wave.

References

[1] G. D. Ferguson, "Blue-green lasers for underwater applications," *Proc. SPIE 0064, Ocean Opt. IV*, vol. 64, pp. 150–156, Nov. 1975.
[2] H. M. Pask, P. Dekker, R. P. Mildren, D. J. Spence, and J. A. Piper, "Wavelength-versatile visible and UV sources based on crystalline Raman lasers," *Prog. Quant. Electron.*, vol. 32, no. 3-4, pp. 121–158, Sep. 2008.

[3] S. Wu, X. Song, and B. Liu, "Fraunhofer lidar prototype in the green spectral region for atmospheric boundary layer observations," *Remote Sens.*, vol. 5, no. 11, pp. 6079–6095, Nov. 2013.
[4] B. Liu, R. Li, Q. Yang, and X. Kong, "Estimation of global detection depth of spaceborne oceanographic lidar in blue-green spectral region," *Infrared Laser Eng.*, vol. 48, no. 1, Jan. 2019, Art. no. 0106006.
[5] S. Tokita, Y. Izawa, H. Niki, and F. Kuwashima, "Selectivity loss due to magnetic field in laser isotope separation of gadolinium based on polarization selection rules," *J. Nucl. Sci. Technol.*, vol. 40, no. 12, pp. 1014–1018, Dec. 2003.
[6] W. Telford *et al.*, "DPSS yellow-green 561-nm lasers for improved fluorochrome detection by flow cytometry," *Cytometry*, vol. 68A, no. 1, pp. 36–44, Jun. 2005.
[7] P. W. Metz *et al.*, "High-power red, orange, and green Pr3+:LiYF$_4$ lasers," *Opt. Lett.*, vol. 39, no. 11, pp. 3193–3196, Jun. 2014.
[8] Y. F. Lü, X. D. Yin, J. Xia, R G Wang, and D Wang, "Efficient continuous-wave intracavity frequency-doubled Nd:YAG-LBO blue laser at 473 nm under diode pumping directly into the emitting level," *Laser Phys. Lett.*, vol. 7, no. 1, pp. 25–28, Jan. 2010.
[9] Y. N. Wang, Q. Zheng, Y. Yao, and X. Chen, "Intracavity sum-frequency diode side-pumped all-solid-state generation yellow laser at 589 nm with an output power of 20.5 W," *Appl. Opt.*, vol. 52, no. 9, pp. 1876–1880, Mar. 2013.
[10] Y. Lu *et al.*, "208 W all-solid-state sodium guide star laser operated at modulated-longitudinal mode," *Opt. Express*, vol. 27, no. 15, pp. 20282–20289, Jul. 2019.
[11] Z. Cong *et al.*, "Theoretical and experimental study on the Nd:YAG/BaWO$_4$/KTP yellow laser generating 8.3 W output power," *Opt. Express*, vol. 18, no. 12, pp. 12111–12118, May 2010.
[12] Q. Sheng *et al.*, "Efficient Nd:YVO4 self-Raman laser in-band pumped by wavelength-locked laser diode at 878.7 nm," *J. Opt.*, vol. 16, no. 10, pp. 1–5, Sep. 2014.
[13] Y. F. Chen, Y. Y. Pan, Y. C. Liu, H. P. Cheng, C. H. Tsou, and H. C. Liang, "Efficient high-power continuous-wave lasers at green-lime-yellow wavelengths by using a Nd:YVO4 self-Raman crystal," *Opt. Express*, vol. 27, no. 3, pp. 2029–2035, Feb. 2019.
[14] Y. Feng, L. R. Taylor, and D. B. Calia, "25 W Raman-fiber-amplifier-based 589 nm laser for laser guide star," *Opt. Express*, vol. 17, no. 21, pp. 19021–19026, Oct. 2009.
[15] S. Rabien, R. I. Davies, T. Ott, S. Hippler, and U. Neumann, "PARSEC: the laser for the VLT," *Proc. SPIE*, vol. 4494, pp. 325–335, Feb. 2002.
[16] T. H. My, C. Drag, and F. Bretenaker, "Single-frequency and tunable operation of a continuous intracavity-frequency-doubled singly resonant optical parametric oscillator," *Opt. Lett.*, vol. 33, no. 13, pp. 1455–1457, Jun. 2008.
[17] O. Mhibik, D. Paboeuf, C. Drag, and F. Bretenaker, "Sub-kHz level relative stabilization of an intracavity doubled continuous wave optical parametric oscillator using Pound-Drever-Hall scheme," *Opt. Express*, vol. 19, no. 19, pp. 18049–18057, Sep. 2011.
[18] G. K. Samanta and M. Ebrahimzadeh, "Continuous-wave, single-frequency, solid-state blue source for the 425–489 nm spectral range," *Opt. Lett.*, vol. 33, no. 11, pp. 1228–1230, Jun. 2008.
[19] R. C. Bapna, C. S. Rao, and K. Dasgupta, "Low-threshold operation of a 355-nm pumped nanosecond β-BaB2O4 optical parametric oscillator," *Opt. Laser Technol.*, vol. 40, no. 6, pp. 832–837, Jan. 2008.
[20] J. Ma, T. Lu, X. Zhu, X. Ma, S. Li, T. Zhou, and W. Chen, "Highly efficient H-β Fraunhofer line optical parametric oscillator pumped by a single-frequency 355 nm laser," *Chin. Opt. Lett.*, vol. 16, no. 8, Aug. 2018, Art. no. 081901.
[21] C. S. Rao, S. Kundu, and A. K. Ray, "High repetition rate nanosecond optical parametric oscillator pumped by the third harmonic of a DPSSL," *Appl. Phys. B*, vol. 124, no. 8, pp. 163, Jul. 2018.
[22] H. Q. Li *et al.*, "High-power nanosecond optical parametric oscillator based on a long LiB3O5 crystal," *Opt. Commun.*, vol. 232, no. 1-6, pp. 411–415, Jan. 2004.
[23] Y. Bi *et al.*, "High-power blue light generation by external frequency doubling of an optical parametric oscillator," *Chin. Phys. Lett.*, vol. 20, no. 11, pp. 1957–1959, Aug. 2003.
[24] G. D. Boyd, A. Ashkin, J. M. Dziedzic, and D. A. Kleinman, "Second-harmonic generation of light with double refraction," *Phys. Rev.*, vol. 137, no. 4A, pp. 1305–1320, Feb. 1965.
[25] SodiumStar – High-power guide star laser @ 589 nm. [Online]. Available: https://www.toptica.com/products/customized-solutions/sodiumstar/
[26] G. T. Moore, K. Koch, and E. C. Cheung. "Optical parametric oscillation with intracavity second-harmonic generation," *Opt. Commun.*, vol. 113, no. 4-6, pp. 463–470, Jan. 1995.
[27] X. Gao, P. Li, Z. Wu, S. Dai, and Y. Gu, "Theoretical analysis of a continuous-wave 323 nm laser generated by a singly resonant optical parametric oscillator with intracavity sum-frequency generation," *Laser Phys.*, vol. 28, no. 8, Jun. 2018, Art. no. 085401.
[28] J. A. Armstrong, N. Bloembergen, J. Ducuing, and P. S. Pershan, "Interactions between light waves in a nonlinear dielectric," *Phys. Rev.*, vol. 127, no. 6, pp. 1918–1939, Apr. 1962.
[29] R. Urschel, A. Borsutzky, and R. Wallenstein, "Numerical analysis of the spatial behaviour of nanosecond optical parametric oscillators of beta-barium borate," *Appl. Phys. B*, vol. 70, no. 2, pp. 203–210, Oct. 2000.
[30] H. Li, A. Geng, Y. Bo, Q. Peng, D. Cui, and Z. Xu, "A 18-W signal average power nanosecond LiB3O5 optical parametric oscillator around 860 nm and the beam quality," *Chin. Phys. Lett.*, vol. 22, no. 7, pp. 1694–1697, Mar. 2005.